Research on Vibration Suppression of Grounded Stiffness Nonlinear Energy Sink

Jiayu Yao

China Railway 19th Bureau Group Corporation Limited, Beijing 100176, China. E-mail: yaojiayu85@163.com

(Received 7 November 2024; accepted 28 April 2025)

Nonlinear energy sinks (NESs) have been widely applied as passive control units in the field of vibration control. In this study, a grounded combined-stiffness NES is proposed, which consists of grounded linear stiffness and grounded cubic stiffness. The vibration suppression performance of the model under different excitations is investigated. First, the slow-varying equations of the system are derived using the complexification-averaging method, followed by the derivation of the amplitude-frequency response equation. Next, the influence of system parameters on vibration reduction performance under harmonic and impulsive excitations is analyzed. Finally, a comparative analysis is conducted on the vibration reduction performance of the grounded linear stiffness NES, grounded cubic stiffness NES, and grounded combined-stiffness NES after parameter optimization using the Grey Wolf Optimizer (GWO) under random excitation. The results indicate that introducing grounded cubic stiffness into the grounded linear stiffness NES can significantly enhance the system's vibration reduction performance. However, compared to the grounded cubic stiffness NES, the energy dissipation of the primary system in the grounded combined-stiffness NES is more sensitive to variations in grounded linear stiffness.

1. INTRODUCTION

Vibration is widespread in mechanical equipment such as machine tools, vehicles, and spacecraft. Prolonged external vibrations can damage structures in engineering, potentially leading to severe consequences. Traditional vibration reduction methods can be classified according to their control strategies into passive control, semi-active control, active control, and hybrid control.[1] Nonlinear energy sinks (NES), known for their high vibration energy dissipation efficiency, good robustness, and small mass,[2,3] have increasingly been applied in vibration suppression for aerospace equipment.[4]

In NES, there exists a phenomenon known as Targeted Energy Transfer (TET), which allows for efficient energy transfer between the auxiliary structure and the primary structure.[5,6] Once TET occurs, energy is irreversibly transferred with minimal or no return to the primary structure, significantly enhancing the system's vibration suppression effect.[7] Ding et al.[8] summarized research on NES and discussed the current state of various types. Mcfarland et al.[9] experimentally validated the presence of TET in grounded cubic NES. Sui et al.[10] proposed a grounded stiffness NES with an inerter and explored the system's dynamic characteristics using the complexification-averaging method, finding that the introduction of an inerter and grounded stiffness effectively improved the vibration reduction performance. Jiang et al.[11] introduced a grounded NES with both cubic stiffness and damping, studying the system's response under harmonic excitation and experimentally confirming that grounded NES offers superior wideband characteristics. Ahmadabadi and Khadem[12] investigated the vibration suppression effects of grounded and ungrounded NES on cantilever beam systems under impulsive excitation, discovering that the optimized system achieved energy dissipation of up to 89%, highlighting the importance of nonlinear normal modes in energy targeted transfer within continuous systems. Charlemagne et al.[13] proposed a grounded cubic stiffness NES and the slow invariant manifold and the strongly modulated response (SMR) of the system are studied based on the complexification-averaging method.

The existing reference has not thoroughly explored the grounded combined stiffness NES, which is composed of grounded linear and cubic stiffness. Therefore, this paper proposes a grounded combined stiffness NES and provides an in-depth analysis of the vibration reduction performance of grounded linear stiffness NES, grounded cubic stiffness NES, and grounded combined stiffness NES under different harmonic, impulsive, and random excitations.

2. SYSTEM MODEL OF GROUNDED STIFFNESS NES

The model of the grounded combined stiffness NES system is shown in Figure 1. Here, m_1 and m_2 represent the masses of the linear primary system and the additional structure, respectively; K_1 is the linear stiffness of the primary system; K_2 denotes the cubic stiffness of the additional structure and the grounded cubic stiffness; K_3 and K_4 are the grounded linear stiffness and grounded cubic stiffness of the additional structure, respectively; c_1 and c_2 are the linear damping coefficients of the primary system and additional structure, respectively; F and ω represent the amplitude and frequency of the external excitation.

The equation of the grounded combined stiffness NES system can be expressed as:

$$\begin{cases} m_1\ddot{X}_1 + C_1\dot{X}_1 + K_1X_1 + \\ K_2\left(X_1 - X_2\right)^3 + C_2\left(\dot{X}_1 - \dot{X}_2\right) = F\cos\omega t \\ m_2\ddot{X}_2 + K_2\left(X_2 - X_1\right)^3 + \\ C_2\left(\dot{X}_2 - \dot{X}_1\right) + K_3X_2 + K_4X_2^3 = 0. \end{cases} \tag{1}$$

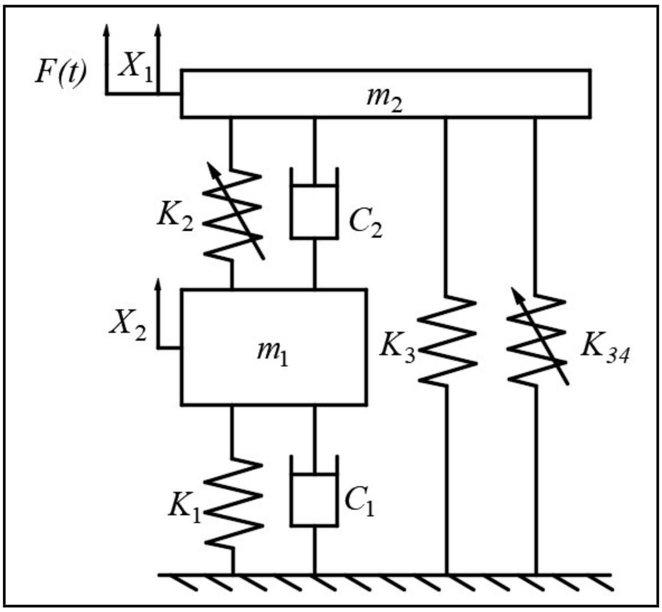

Figure 1. Grounded combined stiffness NES system model.

System 1 may be rescaled as follows:

$$\begin{aligned}
&\omega_0^2=\frac{K_1}{m_1}, \varepsilon\lambda_1=\frac{C_1}{m_1\omega_0}, \varepsilon\lambda_2=\frac{C_2}{m_2\omega_0},\\
&\varepsilon k_2=\frac{l^2K_2}{K_1}, \varepsilon k_3=\frac{K_3}{K_1}, \varepsilon k_4=\frac{l^2K_4}{K_1},\\
&\tau=\omega t, \Omega=\frac{\omega}{\omega_0}, \varepsilon f=\frac{F}{lK_1};
\end{aligned} \tag{2}$$

where τ represents non-dimensional time, l represents the static deformation of the main system spring under the influence of gravity. $0<\varepsilon\ll 1$ is a mall parameter that determines the order of magnitude for damping, amplitude of the external force, detuning, and mass of the attachment.[14] Equation (1) can be expressed in terms of the non-dimensional time scale τ:

$$\begin{cases}
\ddot{x}_1+\varepsilon\lambda_1\dot{x}_1+x_1+\\
\varepsilon\lambda_2\left(\dot{x}_1-\dot{x}_2\right)+\varepsilon k_2\left(x_1-x_2\right)^3=\varepsilon f\cos(\Omega\tau)\\
\ddot{x}_2+\lambda_2\left(\dot{x}_2-\dot{x}_1\right)+\\
k_2\left(x_2-x_1\right)^3+k_3x_2+k_4x_2^3=0.
\end{cases} \tag{3}$$

3. ANALYSIS OF THE VIBRATION REDUCTION PERFORMANCE OF THE SYSTEM UNDER HARMONIC EXCITATION

This section investigates the system's amplitude-frequency response. First, the following variables are introduced to perform a variable substitution in Equation (3).

$$u=x_1+\varepsilon x_2,\ \ v=x_1-x_2. \tag{4}$$

Equation (3) can be transformed into:

$$\begin{cases}
\ddot{u}+\varepsilon\lambda_1\frac{\dot{u}+\varepsilon\dot{v}}{1+\varepsilon}+\frac{u+\varepsilon v}{1+\varepsilon}+\\
\varepsilon k_3\frac{u-v}{1+\varepsilon}+\varepsilon k_4\left(\frac{u-v}{1+\varepsilon}\right)^3=\varepsilon f\cos(\Omega\tau)\\
\ddot{v}+\varepsilon\lambda_1\frac{\dot{u}+\varepsilon\dot{v}}{1+\varepsilon}+\frac{u+\varepsilon v}{1+\varepsilon}+(1+\varepsilon)\lambda_2\dot{v}+(1+\varepsilon)k_2v^3-\\
\varepsilon k_3\frac{u-v}{1+\varepsilon}-\varepsilon k_4\left(\frac{u-v}{1+\varepsilon}\right)^3=\varepsilon f\cos(\Omega\tau).
\end{cases} \tag{5}$$

According to Gendelman, Starosvetsky, Feldman[15] and Starosvetsky, Gendelman[16] introduce the following complex variables:

$$\begin{cases}
\varphi_1e^{j\Omega\tau}=\dot{u}+j\Omega u\\
\varphi_2e^{j\Omega\tau}=\dot{v}+j\Omega v.
\end{cases} \tag{6}$$

From Equation (6), the following relationship can be further obtained:

$$\begin{aligned}
&\ddot{u}=\dot{\varphi}_1e^{j\Omega\tau}+j\Omega\frac{\varphi_1e^{j\Omega\tau}-\bar{\varphi}_1e^{-j\Omega\tau}}{2},\\
&v=\frac{\varphi_2e^{j\Omega\tau}-\bar{\varphi}_2e^{-j\Omega\tau}}{2j\Omega}, \dot{v}=\frac{\varphi_2e^{j\Omega\tau}+\bar{\varphi}_2e^{-j\Omega\tau}}{2}.
\end{aligned} \tag{7}$$

Substituting Equation (7) into Equation (5) and extracting the coefficients of the slow-varying components, the slow-varying equations of the system can be expressed as:

$$\begin{cases}
\dot{\varphi}_1+\frac{j\Omega}{2}\varphi_1+\frac{\varepsilon\lambda_1}{2(1+\varepsilon)}\left(\varphi_1+\varepsilon\varphi_2\right)-\frac{j(\varphi_1+\varepsilon\varphi_2)}{2\Omega(1+\varepsilon)}-\\
\frac{\varepsilon jk_3(\varphi_1-\varphi_2)}{2\Omega(1+\varepsilon)}-\frac{3j\varepsilon k_4\left(|\varphi_1-\varphi_2|^2(\varphi_1-\varphi_2)\right)}{8\Omega^3(1+\varepsilon)^3}=\frac{\varepsilon f}{2}\\
\dot{\varphi}_2+\frac{j\Omega}{2}\varphi_2+\frac{\varepsilon\lambda_1}{2(1+\varepsilon)}\left(\varphi_1+\varepsilon\varphi_2\right)-\\
\frac{j(\varphi_1+\varepsilon\varphi_2)}{2\Omega(1+\varepsilon)}-\frac{3j(1+\varepsilon)k_2}{8\Omega^3}\varphi_2\left|\varphi_2\right|^2+\frac{(1+\varepsilon)\lambda_2}{2}\varphi_2+\\
\frac{\varepsilon jk_3(\varphi_1-\varphi_2)}{2\Omega(1+\varepsilon)}+\frac{3j\varepsilon k_4\left(|\varphi_1-\varphi_2|^2(\varphi_1-\varphi_2)\right)}{8\Omega^3(1+\varepsilon)^3}=\frac{\varepsilon f}{2}.
\end{cases} \tag{8}$$

To obtain the steady-state solution of the system, let $\dot{\varphi}_1=\dot{\varphi}_2=0$, after applying the Euler transformation to $\varphi_1=\beta_1e^{j\gamma_1}$, $\varphi_2=\beta_2e^{j\gamma_2}$ and substituting it into Equation (8), by separating the real and imaginary parts, we have:

$$\begin{cases}
-4f\varepsilon(1+\varepsilon)^3\Omega^3+3\varepsilon k_4\beta_1^3\sin\left(\gamma_1\right)-3\varepsilon\sin\left(\gamma_2\right)k_4\beta_2^3+\\
3\varepsilon k_4\beta_1^2\beta_2\left(\sin\left(2\gamma_1-\gamma_2\right)+2\sin\left(\gamma_2\right)\right)-\\
4\varepsilon(1+\varepsilon)^2\Omega^2\beta_2\left(-\sin\left(\gamma_2\right)\left(k_3-1\right)+\varepsilon\Omega\lambda_1\cos\left(\gamma_2\right)\right)+\\
\beta_1\begin{pmatrix}4\varepsilon(1+\varepsilon)^2\Omega^3\lambda_1\cos\left(\gamma_1\right)+\\4\varepsilon(1+\varepsilon)^2\Omega^2\sin\left(\gamma_1\right)k_3-\\3\varepsilon k_4\beta_2^2\left(-2\sin\left(\gamma_1\right)+\sin\left(\gamma_1-2\gamma_2\right)\right)+\\4(1+\varepsilon)^2\Omega^2\left(-\left(-1+(1+\varepsilon)\Omega^2\right)\sin\left(\gamma_1\right)+\right)\end{pmatrix}=0\\
\\
3\varepsilon k_4\beta_1^2\beta_2\left(\cos\left(2\gamma_1-\gamma_2\right)+2\cos\left(\gamma_2\right)\right)+\\
3\varepsilon k_4\beta_2^3\cos\left(\gamma_2\right)+4\varepsilon(1+\varepsilon)^2\Omega^2\left(k_3-1\right)\beta_2\cos\left(\gamma_2\right)-\\
3\varepsilon k_4\beta_1^3\cos\left(\gamma_1\right)+4\varepsilon^2(1+\varepsilon)^2\Omega^3\lambda_1\Omega\sin\left(\gamma_2\right)+\\
\beta_1\begin{pmatrix}-4\varepsilon(1+\varepsilon)^2\Omega^2k_3\cos\left(\gamma_1\right)-\\3\varepsilon k_4\beta_2^2\left(2\cos\left(\gamma_1\right)+\cos\left(\gamma_1-2\gamma_2\right)\right)+\\4(1+\varepsilon)^2\Omega^2\left(-1+(1+\varepsilon)\Omega^2\right)\cos\left(\gamma_1\right)+\\4\varepsilon(1+\varepsilon)^2\Omega^3\lambda_1\sin\left(\gamma_1\right)\end{pmatrix}=0,
\end{cases}$$

$$\begin{cases}
3\varepsilon k_4\beta_1^2\beta_2\left(\sin\left(2\gamma_1-\gamma_2\right)+2\sin\left(\gamma_2\right)\right)+\\
4\beta_1(1+\varepsilon)^2\Omega^2\left(\sin\left(\gamma_1\right)+\varepsilon\Omega\lambda_1\cos\left(\gamma_1\right)\right)+\\
4(1+\varepsilon)^2\Omega^2\beta_2\left(\varepsilon k_3+\varepsilon-(1+\varepsilon)\Omega^2\right)\sin\left(\gamma_2\right)+\\
4(1+\varepsilon)^2\Omega^3\beta_2\left(\varepsilon^2\lambda_1+(1+\varepsilon)^2\lambda_2\right)\cos\left(\gamma_2\right)+\\
3\beta_1\varepsilon\left(-2\sin\left(\gamma_1\right)+k_4\beta_2^2\sin\left(\gamma_1-2\gamma_2\right)\right)-\\
4\beta_1\varepsilon(1+\varepsilon)^2\Omega^2k_3\sin\left(\gamma_1\right)-3\varepsilon k_4\beta_1^3\sin\left(\gamma_1\right)+\\
3\sin\left(\gamma_2\right)\left(k_2(1+\varepsilon)^4+\varepsilon k_4\right)\beta_2^3-4f\varepsilon(1+\varepsilon)^3\Omega^3=0\\
\\
3\varepsilon k_4\beta_1^3\cos\left(\gamma_1\right)+3\varepsilon\beta_1k_4\beta_2^2\cos\left(\gamma_1-2\gamma_2\right)-\\
3\varepsilon k_4\beta_1^2\beta_2\left(\cos\left(2\gamma_1-\gamma_2\right)+2\cos\left(\gamma_2\right)\right)+\\
4\beta_2(1+\varepsilon)^2\Omega^2\left(\Omega^2+\varepsilon\left(-1+\Omega^2\right)-\varepsilon k_3\right)\cos\left(\gamma_2\right)+\\
\beta_1\begin{pmatrix}4\varepsilon(1+\varepsilon)^2\Omega^2k_3\cos\left(\gamma_1\right)+6\varepsilon\cos\left(\gamma_1\right)+\\4(1+\varepsilon)^2\Omega^2\left(-\cos\left(\gamma_1\right)+\varepsilon\lambda_1\Omega\sin\left(\gamma_1\right)\right)\end{pmatrix}+\\
\beta_2\begin{pmatrix}-3\beta_2^2\left(k_2(1+\varepsilon)^4+\varepsilon k_4\right)\cos\left(\gamma_2\right)+\\4(1+\varepsilon)^2\Omega^3\left(\varepsilon^2\lambda_1+(1+\varepsilon)^2\lambda_2\right)\sin\left(\gamma_2\right)\end{pmatrix}=0.
\end{cases} \tag{9}$$

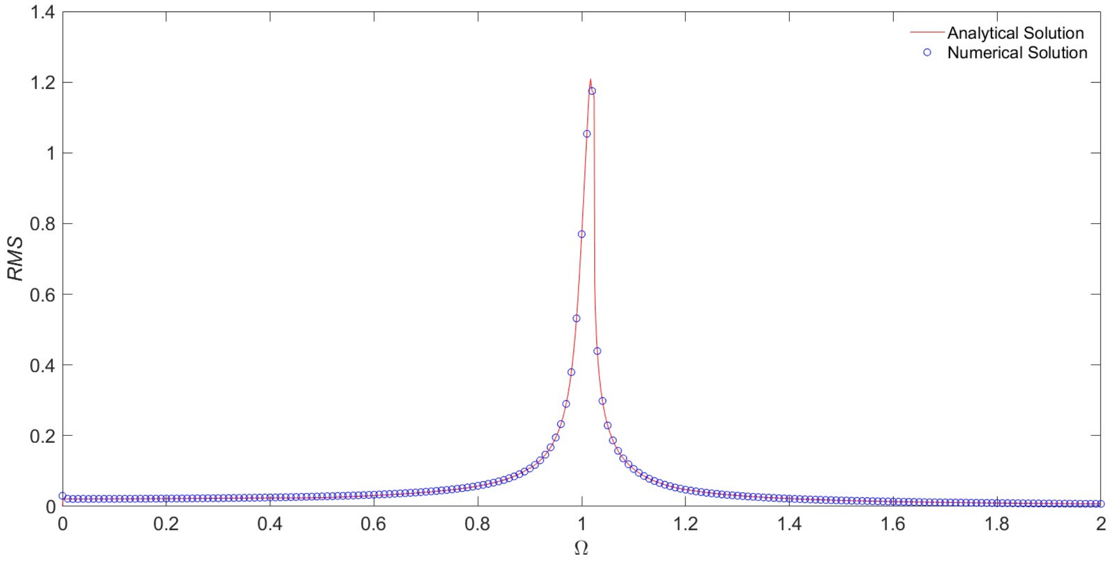

Figure 2. Comparison of the amplitude-frequency response of the system ($\varepsilon = 0.1, \lambda_1 = 0.05, k_2 = 4/3, k_4 = 4/3, f = 0.3$).

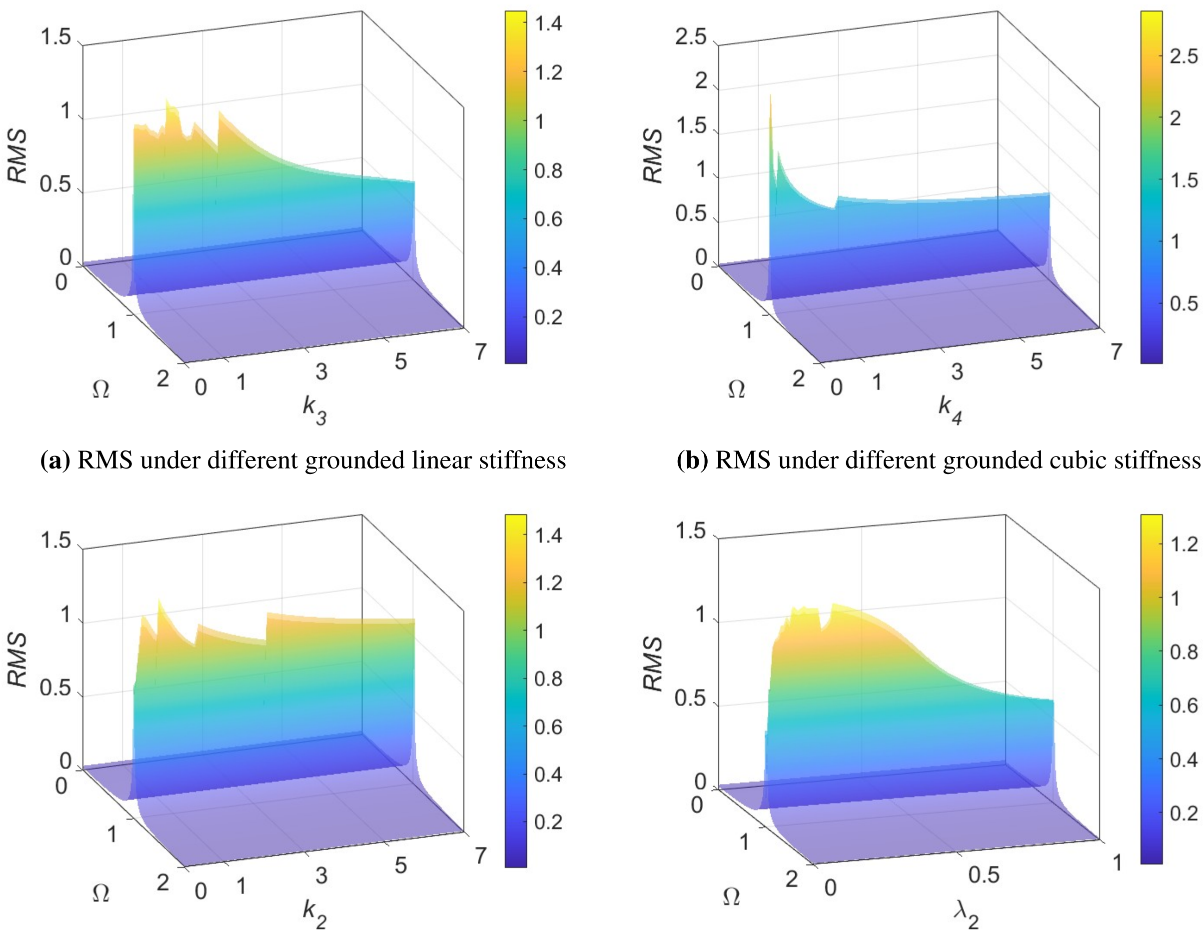

(a) RMS under different grounded linear stiffness

(b) RMS under different grounded cubic stiffness

(c) RMS under different cubic stiffness

(d) RMS under different damping

Figure 3. RMS of the system with different parameters ($\varepsilon = 0.1, \lambda_1 = 0.05, k_2 = 4/3, k_4 = 4/3, f = 0.3$).

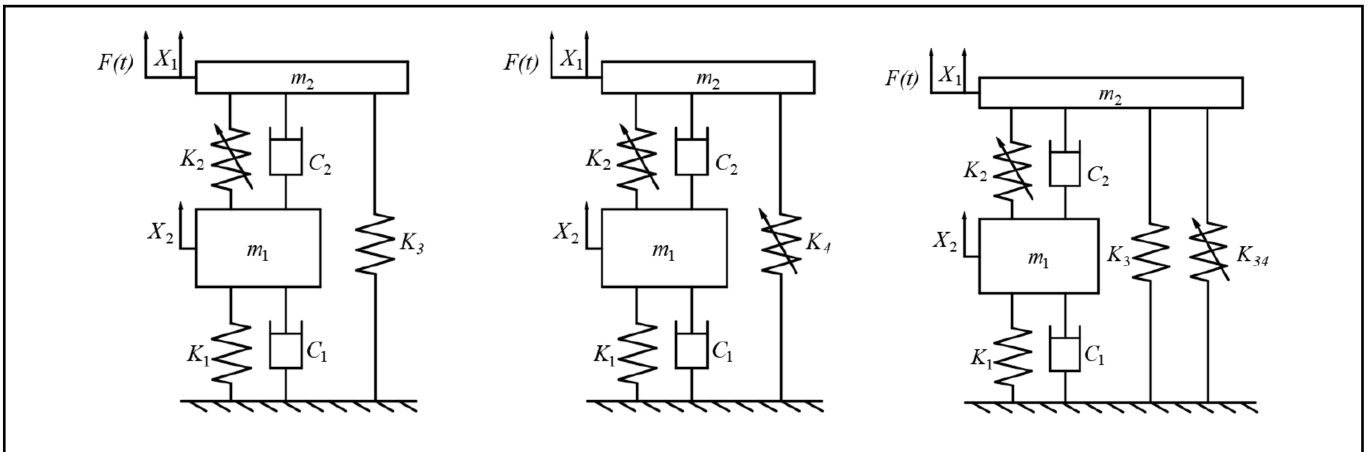

(a) GSK3 (b) GSK4 (c) GSK34

Figure 4. Comparison of different system models.

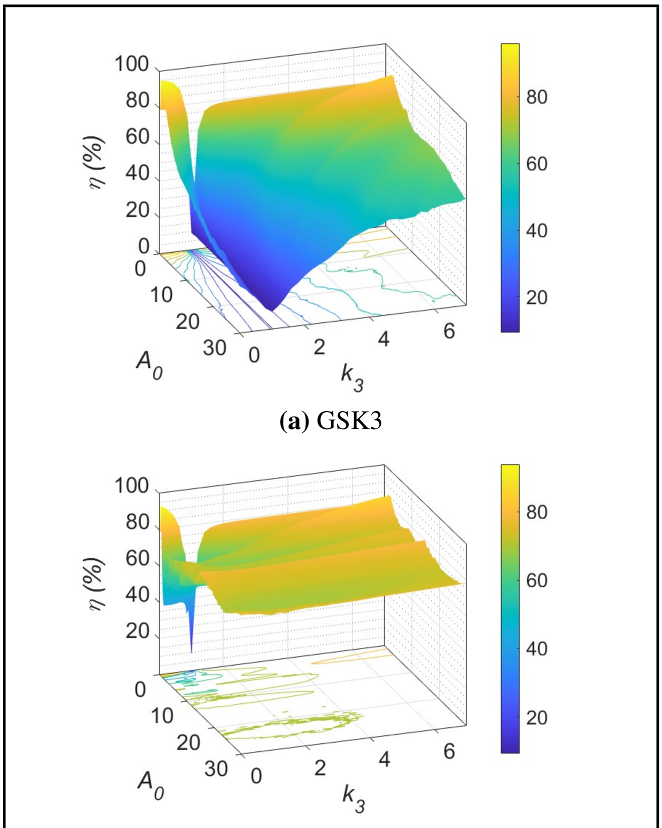

(a) GSK3

(b) GSK34

Figure 5. Energy dissipation ratio of the system under different grounded linear stiffness ($\varepsilon = 0.1, \lambda_1 = 0.05, \lambda_2 = 0.2, k_2 = 4/3, k_4 = 4/3$).

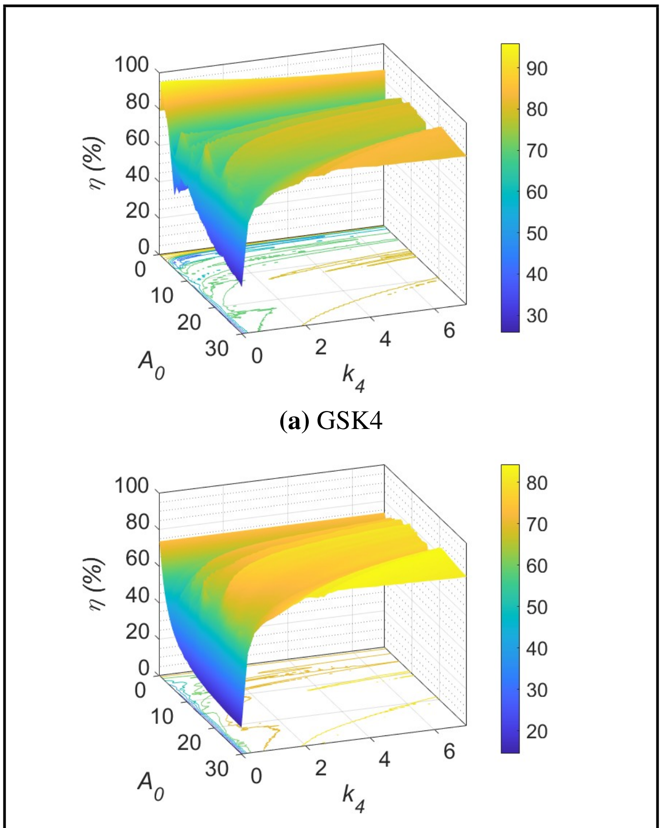

(a) GSK4

(b) GSK34

Figure 6. Energy dissipation ratio of the system under different grounded cubic stiffness ($\varepsilon = 0.1, \lambda_1 = 0.05, \lambda_2 = 0.2, k_2 = 4/3, k_4 = 4/3$).

According to Sui, Shen, Wang[17] the system amplitude can be approximated as follows:

$$\begin{cases} x_1(\tau) \approx \frac{1}{1+\varepsilon}\left(\frac{\beta_1}{\omega}\sin(\Omega\tau+\gamma_1) + \varepsilon\frac{\beta_2}{\omega}\sin(\Omega\tau+\gamma_2)\right) \\ x_2(\tau) \approx \frac{1}{1+\varepsilon}\left(\frac{\beta_1}{\omega}\sin(\Omega\tau+\gamma_1) - \frac{\beta_2}{\omega}\sin(\Omega\tau+\gamma_2)\right). \end{cases} \tag{10}$$

Then the Root Mean Square (RMS) of the steady-state response of the system can be expressed as:

$$\sqrt{\frac{1}{T}\int_0^T [x_i(\tau)]^2\, d\tau}. \tag{11}$$

The comparison between the analytical and numerical solutions of the system's amplitude-frequency response is shown in Figure 2. We can observe that the numerical and analytical solutions fit well, confirming the accuracy of the analytical solution.

To further analyze the influence of parameters on the RMS of the system's amplitude-frequency response. The RMS of the system's amplitude-frequency response under different parameters is shown in Figure 3.

It can be observed that the system's RMS initially increases and then decreases as the grounded linear stiffness increases,

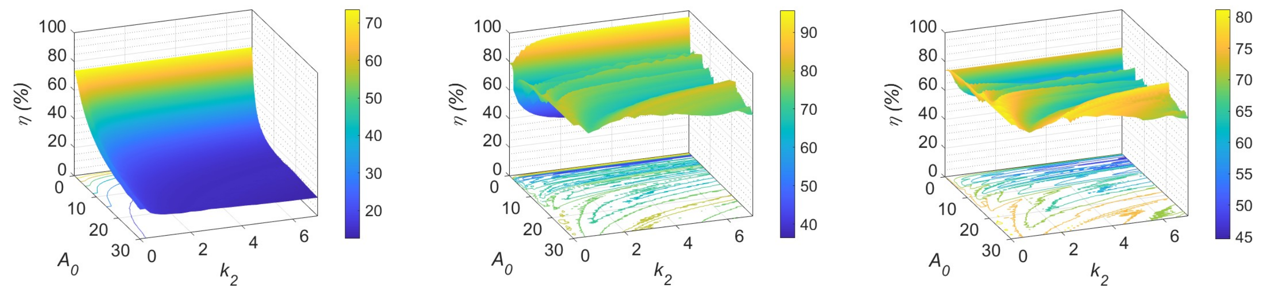

Figure 7. Energy dissipation ratio of the system under different cubic stiffness ($\varepsilon = 0.1, \lambda_1 = 0.05, \lambda_2 = 0.2, k_2 = 4/3, k_4 = 4/3$).

while it gradually decreases with increasing grounded cubic stiffness. As shown in Figure 3(b), introducing grounded cubic stiffness into the grounded linear stiffness NES effectively improves the system's vibration reduction performance. However, when $k_4 > 1.4$ is reached, further increasing the grounded linear stiffness does not significantly enhance the system's vibration reduction performance. Figure 3(c) indicates that when the cubic stiffness is low, the system's amplitude-frequency response RMS is at its minimum, resulting in the best vibration reduction effect. The system can also exhibit good vibration reduction performance when the cubic stiffness is relatively low. Figure 3(d) shows that the system's amplitude-frequency response RMS increases with increasing damping, but beyond a certain level of damping, further increases will reduce the RMS. Therefore, to achieve better vibration reduction performance, it is advisable to select a larger grounded linear stiffness, a relatively larger grounded cubic stiffness, a smaller cubic stiffness, and either low or high damping when designing the system parameters.

4. ANALYSIS OF THE VIBRATION REDUCTION PERFORMANCE OF THE SYSTEM UNDER IMPULSIVE EXCITATION

In this section, we investigate the vibration suppression effects of the system under impulsive excitation and compare the vibration reduction performance of the grounded linear stiffness NES, grounded cubic stiffness NES, and grounded combined stiffness NES under different excitation amplitudes. For ease of discussion, we refer to the grounded linear stiffness NES, grounded cubic stiffness NES, and grounded combined stiffness NES as GSK3, GSK4, and GSK34, respectively, in the subsequent analysis. A comparison of the different system models is shown in Fig. 4.

According to Chen, Zhang, Liu, and Ge,[18] we introduce the energy dissipation ratio η of the primary system.

$$\eta = \frac{E_{LO} - E_{NES}}{E_{LO}}; \tag{12}$$

where, E_{LO} represents the energy of the primary system when the NES is not connected, and E_{NES} represents the energy of the primary system after connecting the NES. The energy dissipation ratios of the system under different grounded linear stiffness, grounded cubic stiffness, and cubic stiffness are shown in Figures 5–7, respectively.

By comparing Figures 5(a) and 5(b), it can be observed that introducing grounded cubic stiffness into GSK3 effectively improves the vibration reduction performance of the system under impulsive excitation. When $A_0 < 1.2$ is reached, the energy dissipation ratios of both GSK3 and GSK34 systems initially decrease and then increase as the grounded linear stiffness increases. However, when $A_0 \geq 1.2$ is reached, the energy dissipation ratio of the GSK34 system with grounded cubic stiffness is significantly higher than that of the GSK3 system. Therefore, incorporating grounded cubic stiffness into the grounded linear stiffness NES can effectively enhance the vibration reduction performance of the system under larger impulsive excitations. Additionally, when the grounded linear stiffness is large, both GSK3 and GSK34 systems exhibit higher energy dissipation ratios under different impulsive excitation amplitudes, indicating better vibration reduction performance at higher grounded linear stiffness.

From Figure 6, it can be seen that the energy dissipation ratios of both GSK4 and GSK34 systems gradually increase with the increase in grounded cubic stiffness. However, compared to grounded cubic stiffness, the energy dissipation ratio of the GSK34 system is more sensitive to changes in grounded linear stiffness. Figure 7 indicates that the energy dissipation ratio of GSK3 sharply decreases with increasing impulsive excitation amplitude, ultimately stabilizing at around 15%. In contrast, GSK34 and GSK4 maintain higher energy dissipation ratios across different impulsive excitation amplitudes.

To further analyze the vibration reduction performance of different systems under impulsive excitation. According to Yang, Wang, Zhang, and Shen,[19] we introduce the difference in energy dissipation ratios η_D, and $\eta_D = \eta_{GDK13} - \eta_{GDKj}, j = 1, 3$. The three-dimensional plots of the differences in energy dissipation ratios among different systems as the system parameters vary are shown in Figure 8, while the proportions $\eta_D \geq 0$ of different systems are presented in Figure 9. For clarity, in the following discussion, the difference in energy dissipation ratios between the GSK34 and GSK3 systems at different grounded linear stiffness values will be referred to as GSK34-3-k3, and the difference between the GSK34 and GSK4 systems at different grounded cubic stiffness values will be referred to as GSK34-4-k4. Similarly, the other differences can be denoted as GSK34-3-k2 and GSK34-4-k2.

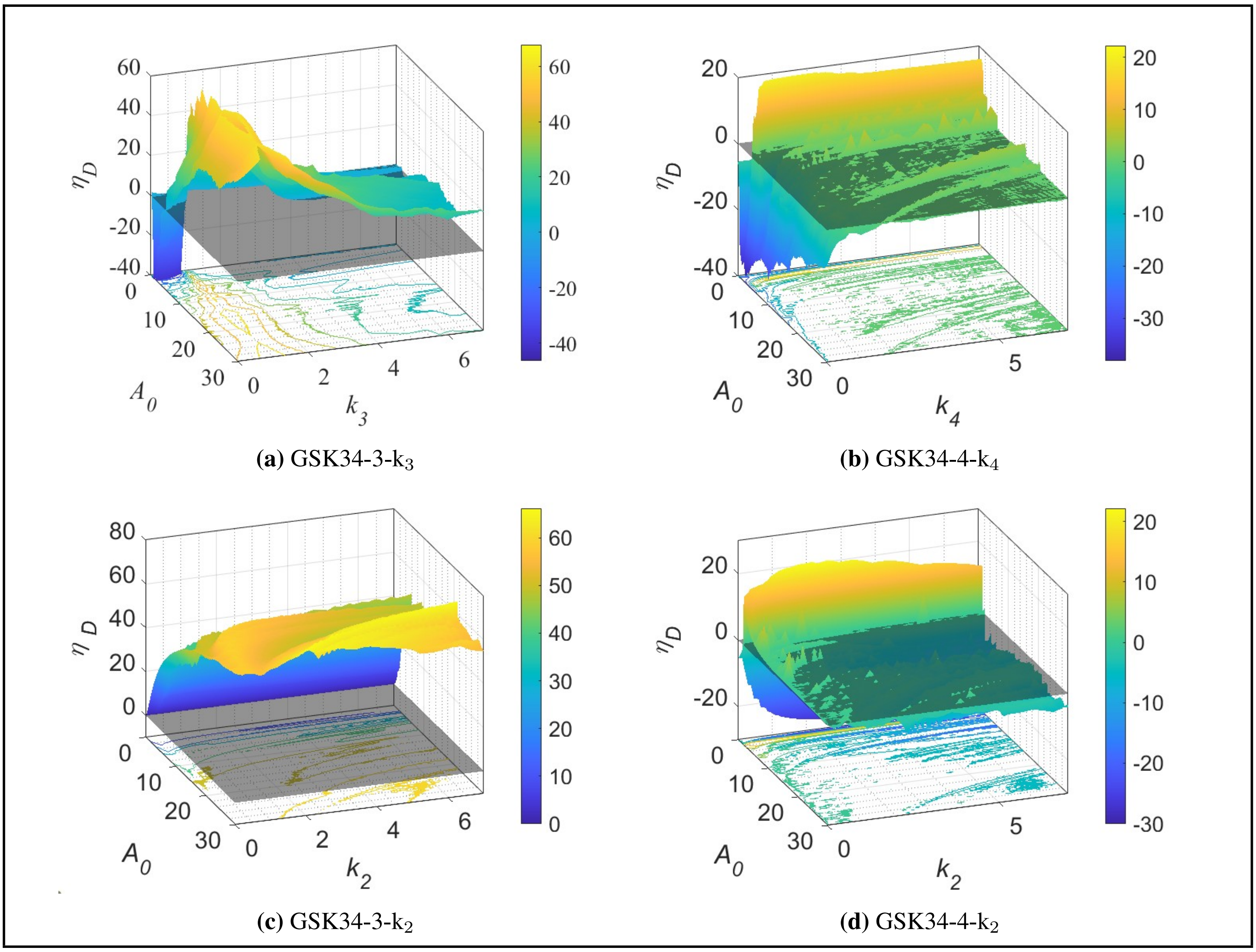

(a) GSK34-3-k_3 **(b)** GSK34-4-k_4

(c) GSK34-3-k_2 **(d)** GSK34-4-k_2

Figure 8. Energy dissipation ratio differences under different parameters.

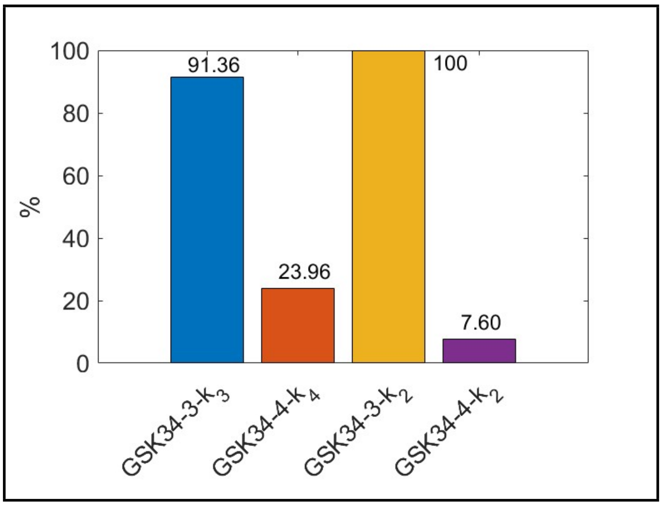

Figure 9. Proportion of $\eta_D \geq 0$ under different system.

From Figure 8(a), it can be observed that when the impulsive excitation amplitude is low ($A_0 < 3$), at smaller grounded linear stiffness ($k_3 < 0.8$), the energy dissipation ratio of GSK34 is much lower than that of GSK3. However, as the grounded linear stiffness increases, the energy dissipation ratio of GSK34 exceeds that of GSK3, reaching a peak difference in energy dissipation ratios when $k_3 = 1$. When the impulsive excitation amplitude is high ($A_0 > 5.3$), the energy dissipation ratio of GSK34 is significantly greater than that of GSK3.

Table 1. Optimal system parameters under different stochastic excitation.

System	D	λ_2	k_2	k_3	k_4	E_S
GSK3	0.2	0.9987	0.4078	10	—	667.7786
GSK4	0.2	0.3795	5.6718	—	0.1063	678.7405
GSK34	0.2	0.9915	0.1588	9.7497	1.9528	660.8430
GSK3	0.5	1	0.1	9.9309	—	4176.1687
GSK4	0.5	0.5356	1.326	—	0.1	4813.0144
GSK34	0.5	1	0.1380	10	9.802	4132.7267
GSK3	1	1	0.1412	10	—	14028.7014
GSK4	1	0.9987	0.1	—	9.3131	19323.7121
GSK34	1	1	0.1889	10	0.7343	14004.7478

Figure 8(b) indicates that when $0.66 \leq A_0 \leq 3.5$, the energy dissipation ratio of GSK34 is significantly higher than that of GSK4. At $A_0 < 0.66$, the energy dissipation ratio of GSK34 is much lower than that of GSK4, but increases with the grounded linear stiffness. When $A_0 > 3.5$, although the energy dissipation ratio of GSK4 is higher than that of GSK34, the difference between the two is not significant.

By examining Figure 8(c) and Figure 9, it can be seen that the difference in energy dissipation ratios between GSK34 and GSK3 is always greater than zero. As indicated in Figure 8(a) and Figure 8(c), this is primarily because the energy dissipation ratio of the GSK3 system sharply decreases with increas-

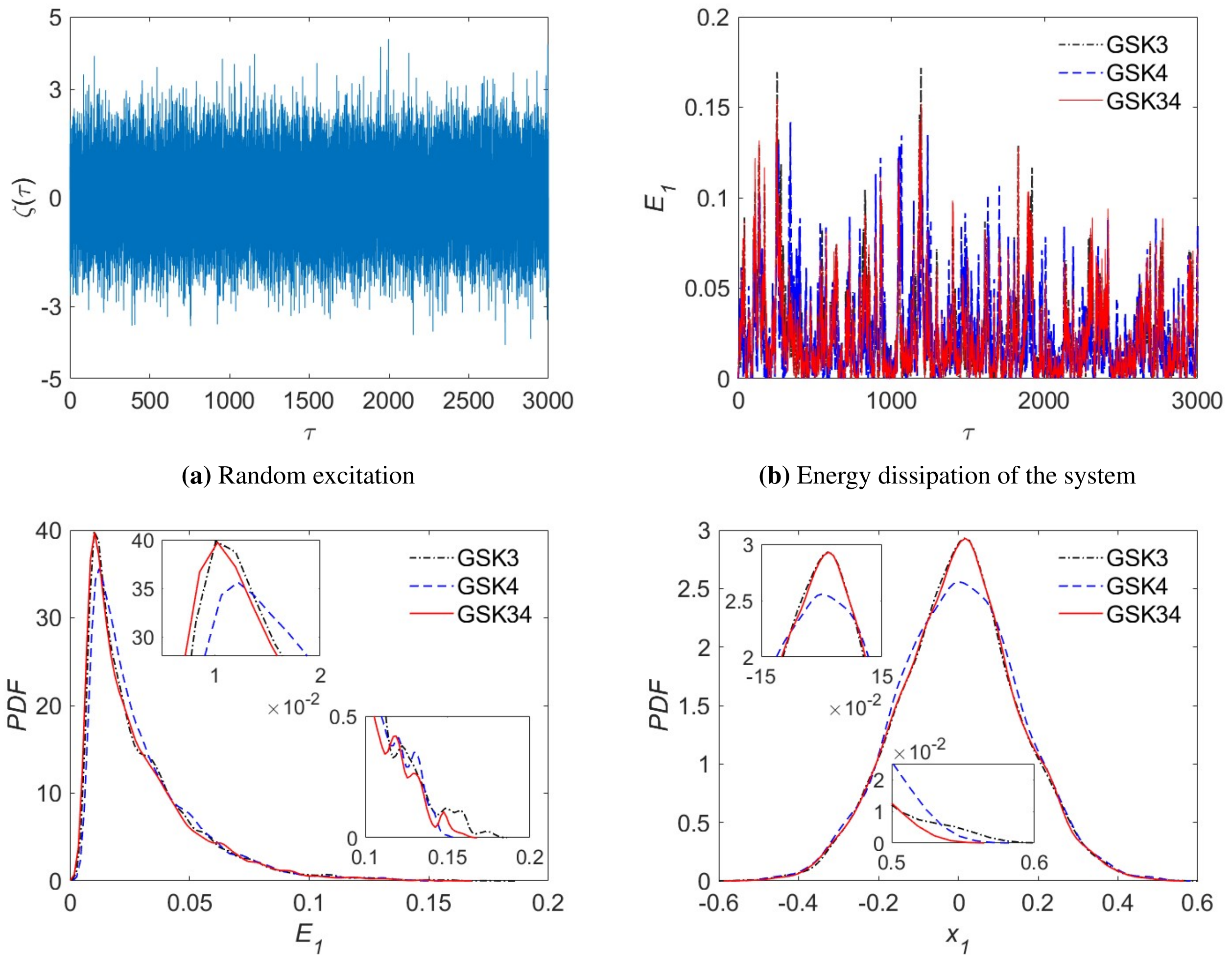

(**a**) Random excitation (**b**) Energy dissipation of the system (**c**) Comparison of primary system energy PDF (**d**) Comparison of system time-history PDF.

Figure 10. $D = 0.2$.

ing impulsive excitation amplitude, while that of the GSK34 system remains at a higher level.

From Figure 8(d), it is noted that when $1.1 \leq A_0 \leq 3.4$, the energy dissipation ratio of GSK34 is greater than that of GSK4, suggesting that under relatively small impulsive excitation amplitudes, GSK34 exhibits better vibration reduction performance compared to GSK4. When $A_0 < 1.1$, the energy dissipation ratio of the GSK34 system is significantly lower than that of GSK4, and as the cubic stiffness increases, the difference in energy dissipation ratios between the two gradually increases. When $A_0 > 3.4$, although the energy dissipation ratio of the GSK4 system is higher than that of GSK34, the difference remains negligible.

5. ANALYSIS OF THE VIBRATION REDUCTION PERFORMANCE OF THE SYSTEM UNDER RANDOM EXCITATION

In complex operating conditions, the system is often subjected to random excitation. In this section, we focus on the vibration reduction performance of the system under random excitation. When the system is subjected to random excitation, the dimensionless differential equations of the system are as follows:

$$\begin{cases} \ddot{x}_1 + \varepsilon\lambda_1\dot{x}_1 + x_1 + \varepsilon\lambda_2\left(\dot{x}_1 - \dot{x}_2\right) + \\ \varepsilon k_2\left(x_1 - x_2\right)^3 = D\zeta(\tau) \\ \ddot{x}_2 + \lambda_2\left(\dot{x}_2 - \dot{x}_1\right) + \\ k_2\left(x_2 - x_1\right)^3 + k_3 x_2 + k_4 x_2^3 = 0. \end{cases}; \quad (13)$$

where, D represents the noise intensity, and $\zeta(\tau)$ denotes Gaussian white noise. Since the system parameters are quite sensitive under random excitation, this paper employs the Grey wolf optimizer (GWO) algorithm to optimize the system parameters under such conditions. The grey wolf algorithm is an intelligent optimization technique that simulates the social hierarchy and hunting behavior of four types of grey wolves.[20] In this study, the area of the primary system's energy under random excitation is used as the objective function, which is optimized using the GWO to minimize this energy area.

The system parameters are set as $\varepsilon = 0.01, \lambda_1 = 0.05$, with the range for the parameters to be optimized set as $\lambda_2 \in [0.01, 1], k_2 \in [1, 10], k_3 \in [1, 10], k_4 \in [1, 10]$. The maximum number of iterations is set to 100, and the wolf population size is set to 30. The optimal parameters for the system under different excitations are shown in Table 1. The optimized probability density curves of the primary system's energy and displacement under various random excitations, along with the

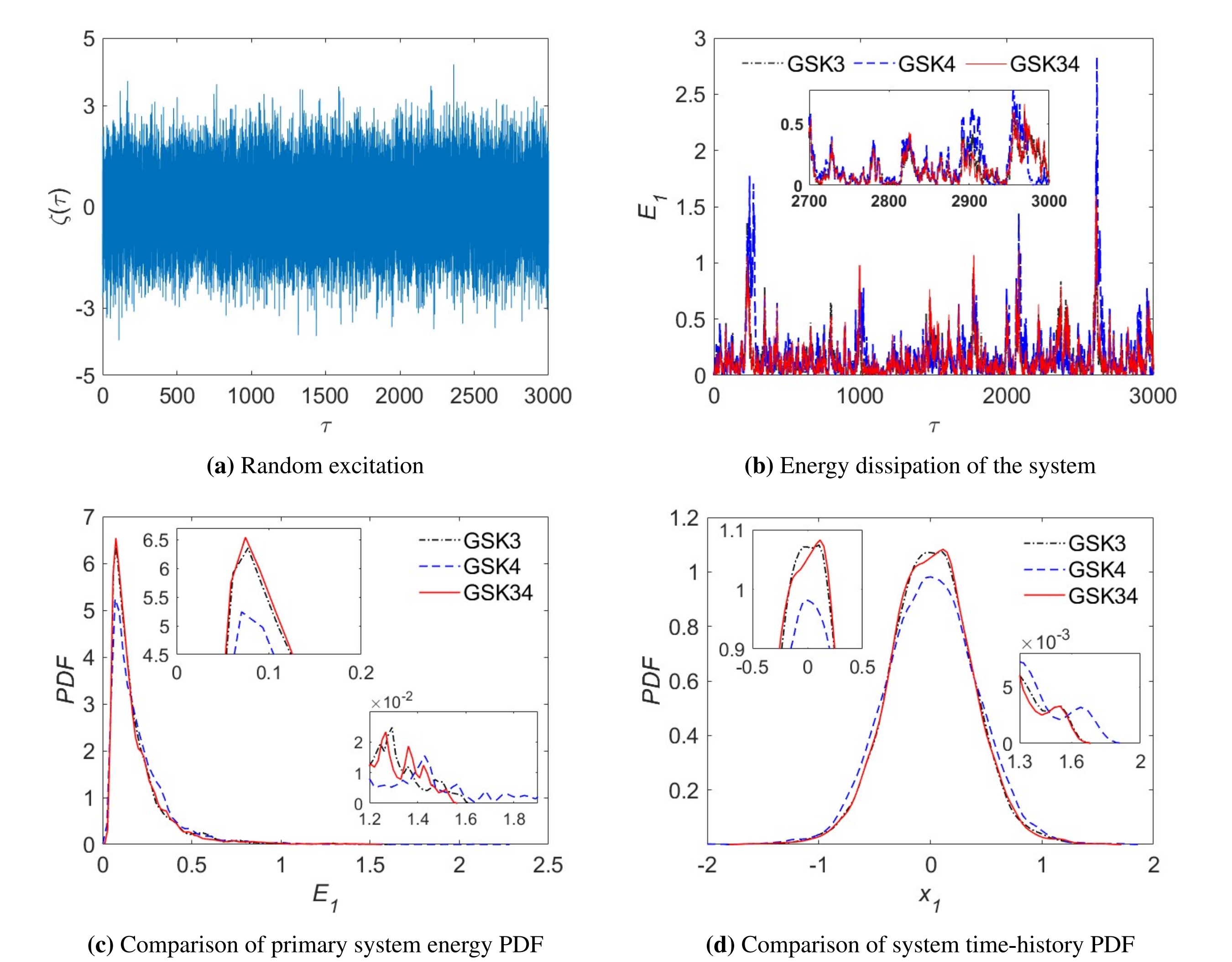

(a) Random excitation (b) Energy dissipation of the system

(c) Comparison of primary system energy PDF (d) Comparison of system time-history PDF

Figure 11. $D = 0.5$.

random excitations themselves, are illustrated in Figures 10–12. Notably, under the same noise intensity D, the random excitations experienced by different systems are the same, while the random excitations vary under different noise intensities.

The system parameters are listed in Table 1. After optimization, the energy dissipation and the probability density function (PDF) of the system are shown in Figures 10–12.

From Figure 10, it can be observed that when the primary system's energy is relatively low, the probability density of the GSK34 system is the highest, indicating that under smaller random excitations, the probability of the GSK34 system having low energy $(E_1 < 0.01)$ is maximized, resulting in the best vibration reduction performance. However, the probability density of the GSK3 system is generally similar to that of GSK34, suggesting that under smaller random excitations, the difference in vibration reduction performance between GSK3 and GSK34 is minimal. The peak probability density of GSK4 is lower than that of both GSK3 and GSK34. Additionally, the peak probability density shifts to the right, indicating that under smaller random excitations, the probability of the GSK4 system having low energy is higher, leading to better vibration reduction performance.

From Figures 11 and 12, it can be observed that, similar to the case under low-intensity random excitations, the vibration reduction performance of the optimized GSK4 system is inferior to that of the GSK3 and GSK34 systems. Moreover, as the amplitude of the random excitation D increases, the performance gap between GSK4 and the other two systems becomes more pronounced. Additionally, although GSK34 exhibits a higher probability density than GSK3 when the primary system's energy is low, the difference between them is not significant. These results suggest that while introducing grounded cubic stiffness into the grounded linear stiffness NES can improve the vibration reduction performance under random excitation, the improvement is relatively limited.

6. CONCLUSIONS

This study investigated the vibration reduction performance of grounded linear stiffness NES, grounded cubic stiffness NES, and grounded combined stiffness NES under different types of excitation. The findings are summarized as follows:

Under harmonic excitation, better vibration reduction performance can be achieved by selecting a larger grounded linear stiffness, a relatively larger grounded cubic stiffness, a smaller cubic stiffness coefficient, and either a smaller or larger damping value during system parameter design.

Under impulsive excitation, introducing grounded cubic stiffness into the grounded linear stiffness NES can effectively

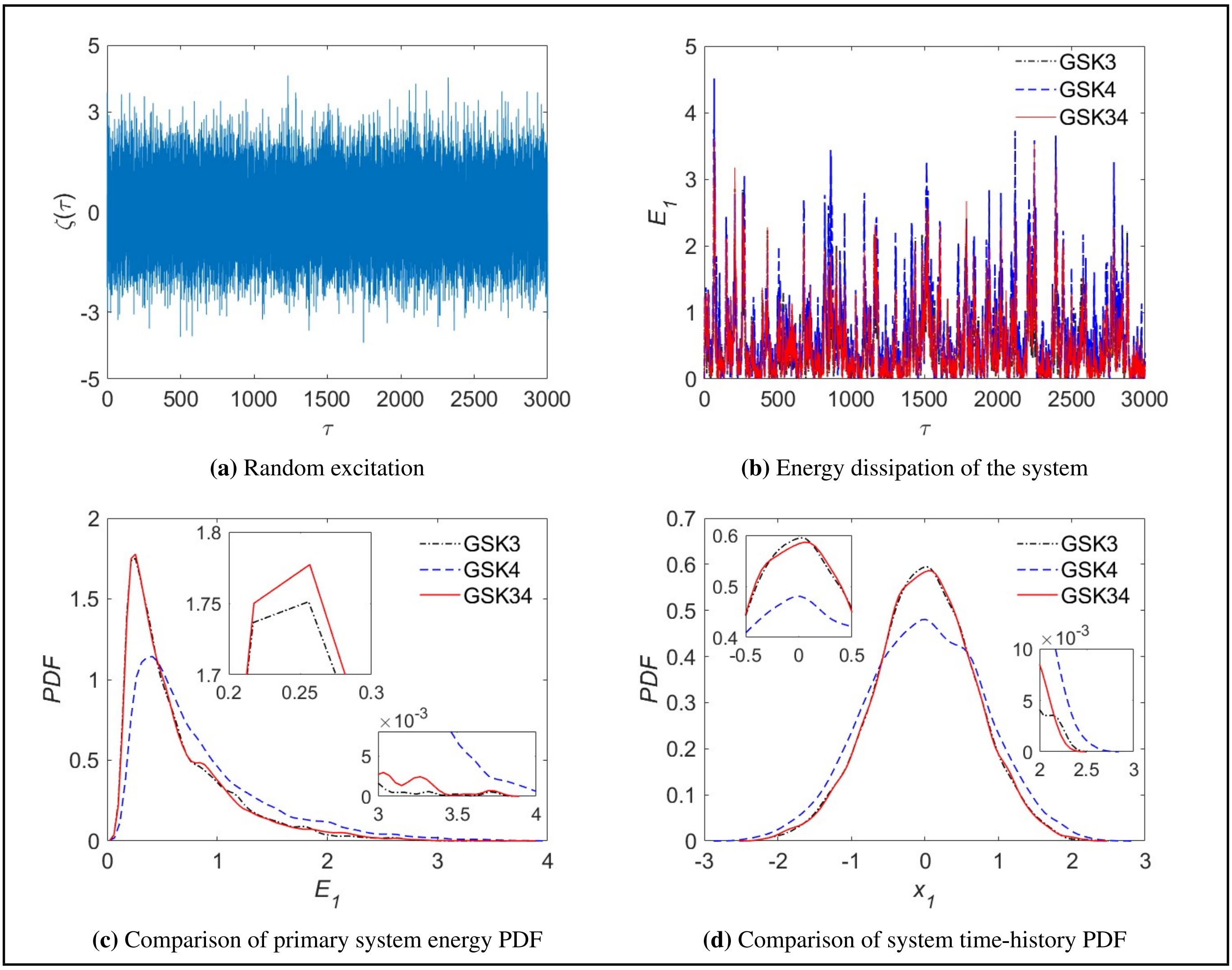

(a) Random excitation

(b) Energy dissipation of the system

(c) Comparison of primary system energy PDF

(d) Comparison of system time-history PDF

Figure 12. $D = 1$.

improve the system's vibration reduction performance. However, compared to the grounded cubic stiffness NES, the energy dissipation ratio of the main system in the grounded combined stiffness NES was more sensitive to variations in grounded linear stiffness. Therefore, relatively small grounded linear stiffness values should be avoided during parameter design to ensure effective vibration reduction.

combined stiffness NES exhibited the best vibration reduction performance, followed by the grounded linear stiffness NES, while the grounded cubic stiffness NES showed the poorest performance. Although incorporating grounded cubic stiffness into the grounded linear stiffness NES can improve the system's performance under random excitation, the improvement is not substantial.

REFERENCES

[1] Lu Z. and Chen, L. Some recent progresses in nonlinear passive isolations of vibrations, *Chinese Journal of Theoretical and Applied Mechanics*, **49**(3), 550–564, (2017). https://doi.org/10.6052/0459-1879-17-064

[2] Vakakis, A. F. Inducing passive nonlinear energy sinks in vibrating systems, *J. Vib. Acoust.*, **123**(3), 324–332, (2001). https://doi.org/10.1115/1.1368883

[3] Vakakis, A. F. and Gendelman, O. Energy pumping in nonlinear mechanical oscillators: part II—resonance capture, *J. Appl. Mech.*, **68**(1), 42–48, (2001). https://doi.org/10.1115/1.1345525

[4] Liu, H., Wang, Y., and Shi, W. Vibration suppression for a flywheel based on nonlinear energy sink, *Journal of Astronautics*, **38**(5), 490, (2017). https://doi.org/10.3873/j.issn.1000-1328.2017.05.007

[5] Kopidakis, G., Aubry, S., and Tsironis, G. P. Targeted energy transfer through discrete breathers in nonlinear systems, *Physical Review Letters*, **87**(16), 165501, (2001). https://doi.org/10.1103/PhysRevLett.87.165501

[6] Saeed, A. S., Al-Shudeifat, M. A., Cantwell, W. J., and Vakakis, A. F. Two-dimensional nonlinear energy sink for effective passive seismic mitigation, *Communications in Nonlinear Science and Numerical Simulation*, **99**, 105787, (2021). https://doi.org/10.1016/j.cnsns.2021.105787

[7] Lu, Z., Wang, Z., and Lv, X. A review on nonlinear energy sink technology, *Journal of Vibration and Shock*, **39**(4), 1–16, (2020). https://doi.org/10.13465/j.cnki.jvs.2020.04.001

[8] Ding, H. and Chen, L. Q. Designs, analysis, and applications of nonlinear energy sinks, *Nonlinear Dynamics*, **100**(4), 3061–3107, (2020). https://doi.org/10.1007/s11071-020-05724-1

[9] McFarland, D. M., Bergman, L. A., and Vakakis, A. F. Experimental study of non-linear energy pumping occurring at a single fast frequency, *International Journal of Non-Linear Mechanics*, **40**(6), 891–899, (2005). https://doi.org/10.1016/j.ijnonlinmec.2004.11.001

[10] Sui, P., Shen, Y., and Wang, X. Study on response mechanism of nonlinear energy sink with inerter and grounded stiffness, *Nonlinear Dynamics*, **111**(8), 7157–7179, (2023). https://doi.org/10.1007/s11071-022-08226-4

[11] Jiang, X., McFarland, D. M., Bergman, L. A., and Vakakis, A. F. Steady state passive nonlinear energy pumping in coupled oscillators: theoretical and experimental results, *Nonlinear Dynamics*, **33**, 87–102, (2003). https://doi.org/10.1023/A:1025599211712

[12] Ahmadabadi, Z. N. and Khadem, S. E. Nonlinear vibration control of a cantilever beam by a nonlinear energy sink, *J. Mechanism and Machine Theory*, **50**, 134–149, (2012). https://doi.org/10.1016/j.mechmachtheory.2011.11.007

[13] Charlemagne, S., Lamarque, C. H., and Savadkoohi, A. T. Dynamics and energy exchanges between a linear oscillator and a nonlinear absorber with local and global potentials, *Journal of Sound and Vibration*, **376**, 33–47, (2016). https://doi.org/10.1016/j.jsv.2016.03.018

[14] Starosvetsky, Y. and Gendelman, O. V. Strongly modulated response in forced 2DOF oscillatory system with essential mass and potential asymmetry, *Physica D: Nonlinear Phenomena*, **237**(13), 1719–1733, (2008). https://doi.org/10.1016/j.physd.2008.01.019

[15] Gendelman, O. V., Starosvetsky, Y., and Feldman, M. Attractors of harmonically forced linear oscillator with attached nonlinear energy sink I: description of response regimes, *Nonlinear Dynamics*, **51**, 31–46, (2008). https://doi.org/10.1007/s11071-006-9167-0

[16] Starosvetsky, Y. and Gendelman, O. V. Response regimes of linear oscillator coupled to nonlinear energy sink with harmonic forcing and frequency detuning, *Journal of Sound and Vibration*, **315**(3), 746–765, (2008). https://doi.org/10.1016/j.jsv.2007.12.023

[17] Sui, P., Shen, Y., and Wang, X. Similarities and differences between the complexification-averaging method and other approximation methods, *Journal of Vibration and Shock*, **42**(10), 289–296, (2023). https://doi.org/10.13465/j.cnki.jvs.2023.10.034

[18] Chen, J., Zhang, W., Liu, J., and Ge, W. Vibration reduction efficiency and damping connection type of multi-scale series nonlinear energy sinks, *Journal of Vibration and Shock*, **41**(10), 147–153, (2022). https://doi.org/10.13465/j.cnki.jvs.2022.10.019

[19] Yang, Z., Wang, J., Zhang, J., and Shen, Y. Research on dynamics characteristics of grounded damping nonlinear energy sink, *International Journal of Structural Stability and Dynamics*, 2550156, (2024). https://doi.org/10.1142/S0219455425501561

[20] Mirjalili, S., Mirjalili, S. M., and Lewis, A. Grey wolf optimizer, *Advances in Engineering Software*, **69**, 46–61, (2014). https://doi.org/10.1016/j.advengsoft.2013.12.007